RESEARCH ARTICLE

ARCTIC OCEANOGRAPHY

Greater role for Atlantic inflows on sea-ice loss in the Eurasian Basin of the Arctic Ocean

Igor V. Polyakov,[1]* Andrey V. Pnyushkov,[2] Matthew B. Alkire,[3] Igor M. Ashik,[4] Till M. Baumann,[1] Eddy C. Carmack,[5] Ilona Goszczko,[6] John Guthrie,[3] Vladimir V. Ivanov,[7,8,4] Torsten Kanzow,[9,10] Richard Krishfield,[11] Ronald Kwok,[12] Arild Sundfjord,[13] James Morison,[3] Robert Rember,[2] Alexander Yulin[4]

Arctic sea-ice loss is a leading indicator of climate change and can be attributed, in large part, to atmospheric forcing. Here, we show that recent ice reductions, weakening of the halocline, and shoaling of the intermediate-depth Atlantic Water layer in the eastern Eurasian Basin have increased winter ventilation in the ocean interior, making this region structurally similar to that of the western Eurasian Basin. The associated enhanced release of oceanic heat has reduced winter sea-ice formation at a rate now comparable to losses from atmospheric thermodynamic forcing, thus explaining the recent reduction in sea-ice cover in the eastern Eurasian Basin. This encroaching "atlantification" of the Eurasian Basin represents an essential step toward a new Arctic climate state, with a substantially greater role for Atlantic inflows.

Over the past decade, the Arctic Ocean has experienced dramatic sea-ice loss in the summers, with record-breaking years in 2007 and 2012 for both the Amerasian Basin and the Eurasian Basin (EB). More remarkably, the eastern EB has been nearly ice-free (<10% ice coverage) at the end of summer since 2011 (Fig. 1). Most sea-ice-mass loss results from summer solar heating of the surface mixed layer (SML) through cracks in the ice and open water, and consequent melting of the lower surface of the ice (*1*–*3*). Heat advected into the EB interior by Atlantic water (AW) generally has not been considered an important contributor to sea-ice reduction, due to effective insulation of the overlying cold halocline layer (CHL) (*4*) that separates the cold and fresh SML and pack ice from heat carried by the warm and saline AW.

There are, however, reasons to believe the role of AW heat in sea-ice reduction is not negligible and may be increasingly important (*5*). Nansen (*6*) identified the importance of warm (temperature >0°C) and salty intermediate-depth (150 to 900 m) AW in establishing the thermal state of the Arctic Ocean. Later studies demonstrated that AW is transported cyclonically (counterclockwise) along the deep Arctic Basin margins (*7*–*10*), carrying enough heat, if released, to melt the Arctic sea ice many times over. Observations from the 1990s and 2000s documented two warm, pulse-like AW temperature anomalies on the order of 1°C (relative to the 1970s), entering the Arctic through Fram Strait and occupying large areas of the Arctic Ocean (*11*–*14*). The strength of the 2000s warming peaked in 2007–2008, with no analogy since the 1950s (*14*). This AW warming has slowed slightly since 2008 (Fig. 2C).

Strong stratification, which is found in most of the Arctic Ocean, prevents vigorous ventilation of the AW. One notable exception is the western Nansen Basin, north and northeast of Svalbard, where proximity to the sources of inflowing AW makes possible strong interactions between the SML and the ocean interior (*5*). Specifically, weakly stratified AW entering the Nansen Basin through Fram Strait is subject to direct ventilation in winter, caused by cooling and haline convection associated with sea-ice formation (*15*). This ventilation leads to the reduction of sea-ice thickness along the continental slope off Svalbard (*16*, *17*). In the past, these conditions have been limited to the western EB, because winter ventilation of AW in the eastern EB was constrained by stronger stratification there. However, newly acquired data show that conditions previously only identified in the western Nansen Basin now can be observed in the eastern EB as well. We call this eastward progression of the western EB conditions the "atlantification" of the EB of the Arctic Ocean.

Overview of sea-ice state

The progressive decline in sea-ice coverage of the Arctic Ocean during the satellite era, at 13.4% per decade during September (*18*), has been accompanied by decreases in average sea-ice thickness of at least 1.7 m in the central Arctic (*19*, *20*). In the region of the eastern EB defined by the polygon in Fig. 1A, the local changes since 2003 have also been substantial. With the northward retreat of multiyear sea-ice cover (*21*), coverage within that polygon is now dominated by seasonal ice, either advected from the east and south or produced locally. Mean September ice coverage has been <10% of the total area during the past 5 years, portending ice-free summers in coming years if current sea-ice trends prevail. Annual open-water coverage has increased from less than 1 month to more than 3 months in recent years (Fig. 1B); these longer ice-free periods, maintained by atmospheric and ocean conditions, increase direct air-ocean interactions (momentum and energy exchanges). Available satellite estimates of ice thickness in this region—typically sparse—suggest a concurrent trend, leading to an overall thinning of ~0.5 m (in March) from 2003 through 2015 (Fig. 1C). Satellite records show that this pattern continued in 2016, with less extensive (compared with record minimum) December sea-ice extent in the Kara and Barents Seas (*22*).

Role of atmospheric thermodynamics in sea-ice decline

Arctic-wide warming is evident from surface air temperature trends ranging between 0.1° and 0.3°C per decade for the period 1984 to 2012 (*23*). Surface air temperature trends from weather stations and ERA-Interim reanalysis data for the Laptev Sea and eastern EB region far exceed observed average Arctic regional trends (fig. S1, A to C), consistent with recently enhanced sea-ice decline. The net atmospheric thermodynamic effect on sea ice cannot be quantified using surface air temperature records alone, because changes in this parameter omit thermodynamic forcing due to additional atmospheric processes.

Fortunately, records are available for fast-ice (motionless seasonal sea ice anchored to the shore, which melts and refreezes each year) thickness, providing a measure of nearly pure atmospheric thermodynamic forcing over the broad, shallow Siberian shelves, where the effect of advected or seasonally stored oceanic heat is negligible. Records

[1]International Arctic Research Center and College of Natural Science and Mathematics, University of Alaska Fairbanks, 930 Koyukuk Drive, Fairbanks, AK 99775, USA. [2]International Arctic Research Center, University of Alaska Fairbanks, 930 Koyukuk Drive, Fairbanks, AK 99775, USA. [3]Polar Science Center, Applied Physics Laboratory, University of Washington, 1013 Northeast 40th Street, Seattle, WA 98105, USA. [4]Arctic and Antarctic Research Institute, 38 Bering Street, Saint Petersburg 199397, Russia. [5]Institute of Ocean Sciences, Fisheries and Oceans Canada, 9860 West Saanich Road, Sidney, BC, V8L 4B2, Canada. [6]Institute of Oceanology, Polish Academy of Sciences, Powstancow Warszawy 55, 81-712 Sopot, Poland. [7]International Arctic Research Center, University of Alaska Fairbanks, 930 Koyukuk Drive, Fairbanks, AK, 99775, USA. [8]Hydrometeorological Center of Russia, 11-13, B, Predtechensky Pereulok, Moscow, 123242, Russia. [9]Alfred-Wegener-Institute, Helmholtz Centre for Polar and Marine Research, Bussestraße 24, 27570 Bremerhaven, Germany. [10]Department of Physics and Electrical Engineering, Bremen University, Otto-Hahn Allee, 28334 Bremen, Germany. [11]Woods Hole Oceanographic Institution, 22 Water Street, Woods Hole, MA 02543, USA. [12]Jet Propulsion Laboratory, California Institute of Technology, 4800 Oak Grove Drive Pasadena, CA 91109, USA. [13]Norwegian Polar Institute, Fram Centre, N-9296 Tromsø, Norway.
*Corresponding author. Email: igor@iarc.uaf.edu

from five locations along the Laptev Sea coast (fig. S1E) have been used to construct a composite time series showing that increased melting in the eastern EB/Laptev Sea region during the past decade accounted for ~18 cm of ice thickness loss (fig. S1D). This estimate is statistically significant at the 95% level (using Student's *t* test) and suggests that atmospheric thermodynamic forcing plays an important role in reducing EB sea-ice coverage.

Recent "atlantification" of the Eurasian Basin

Observations from 2013 to 2015 using oceanographic moorings (fig. S2) and drifting Ice-Tethered Profiler buoys (ITPs) (*3*, *24*) provide evidence that the eastern EB is in a transition to conditions similar to the western Nansen Basin. Mooring observations over the central Laptev Sea slope sustained since 2002 reveal anomalously strong seasonal signals in the subsurface layers during recent years (Fig. 2C and fig. S3). In particular, the enhanced seasonal signals in the winters of 2013–2014 and 2014–2015 are associated with warming (Fig. 2, B and C) and shoaling of the AW layer (Fig. 2, B and D) and weakening of the stability of the CHL and upper pycnocline (~50 to 150 m) (Fig. 2B). As a result, the strength of the seasonal signal, as shown by wavelet analyses (Fig. 2D and fig. S3), was intensified. The AW layer's seasonal temperature range at the $M1_4$ mooring site increased from 0.2° to 0.3°C in 2004 to 2007 (*25*) to over 1°C in 2013 to 2015 (Fig. 2B). Shoaling of the AW upper boundary was also substantial, rising from 140 m in 2003–2004 to 100 m in winter 2014–2015 and even to 85 m in winter 2013–2014 (Fig. 2D), with direct consequences for winter entrainment of AW in the upper ocean.

Observations from the widely distributed array of moorings and ITPs can be used to place measurements from the $M1_4$ mooring location in a basin-wide context (Fig. 3). Temperature and salinity distributions provided by ITP-93, which drifted along the Lomonosov Ridge separating the Amerasian and Eurasian basins, are distinct from those provided by other instruments (Fig. 3). They show a stable SML and CHL (white and black lines in Fig. 3C; see the supplementary materials for SML and CHL depth definitions), and lack strong depth variability throughout the record. The ITP-93 record shows high values for Brunt-Väisälä frequency (a measure of water-column stability) at roughly 25- to 50-m depth from the beginning (22 September 2015) to the end (22 April 2016) of the record, thus providing further evidence for minimal mixing along the eastern flank of the EB in recent years (Fig. 3C).

ITP-57 drifted within the central Amundsen Basin in 2013. Its record shows, in contrast, clear signs of winter ventilation associated with gradual cooling and erosion of the CHL from November/December through April, weakening stratification at the base of the SML, and a decrease in Brunt-Väisälä frequency in the CHL during March and April of 2013 (Fig. 3D). Data from ITP-37 (not shown), which drifted in the same region in 2009–2010, indicated that the transfer of heat from the upper pycnocline (~65 to 100 m) to the SML is highest in winter, with an average heat loss of 3 to 4 W m^{-2} between January and April (*14*). This analysis has also suggested that the increased heat transfer from the AW to the SML in winter is likely caused by a combination of brine-driven convection, associated with sea-ice formation and larger vertical velocity shear below the base of the SML, which is enhanced by strong winter storms and a more mobile ice cover.

A year-long 2013–2014 ITP-74 record from the central Nansen Basin showed deepening of the SML to ~130 m and disappearance of the CHL driven by winter convection in March–April 2014, when the buoy was passing westward to the north of Franz Josef Land (Fig. 3B). A seasonally ventilated halocline was also found in this region on a Russian ice drift station NP-35 in 2007–2008 (*5*) and in earlier observations (*26*, *27*). The disappearance of the CHL was also observed in the central Amundsen Basin in the mid-1990s (*28*). This was explained by a deficit of fresh water in the region, due to a diversion of Siberian river waters further eastward along the coast that was driven by changes in the atmospheric circulation.

The deep winter ventilation and the disappearance of the CHL in the eastern EB (eastward from Severnaya Zemlya, >90°E) at several mooring sites in 2013 to 2015, however, are unprecedented (Figs. 3A and 4). Substantial changes in seasonal heat content *Q* (see definition in the supplementary materials), driven by surface cooling and salinification during winter sea-ice formation, occurred in the upper 130-m layer at M3e, $M1_3$, $M1_6$, and M6b mooring sites. If this trend persists, convectively driven winter development of the deep (>80 m) SML, combined with ventilation of the upper 130-m ocean and associated disappearance of the CHL would represent a fundamental change, with the eastern EB water-column structure becoming less stratified and susceptible to further mixing.

Role of oceanic heat in sea-ice decline

Figure 4 addresses the consequences of these changes for upward AW heat transfer. Seasonal

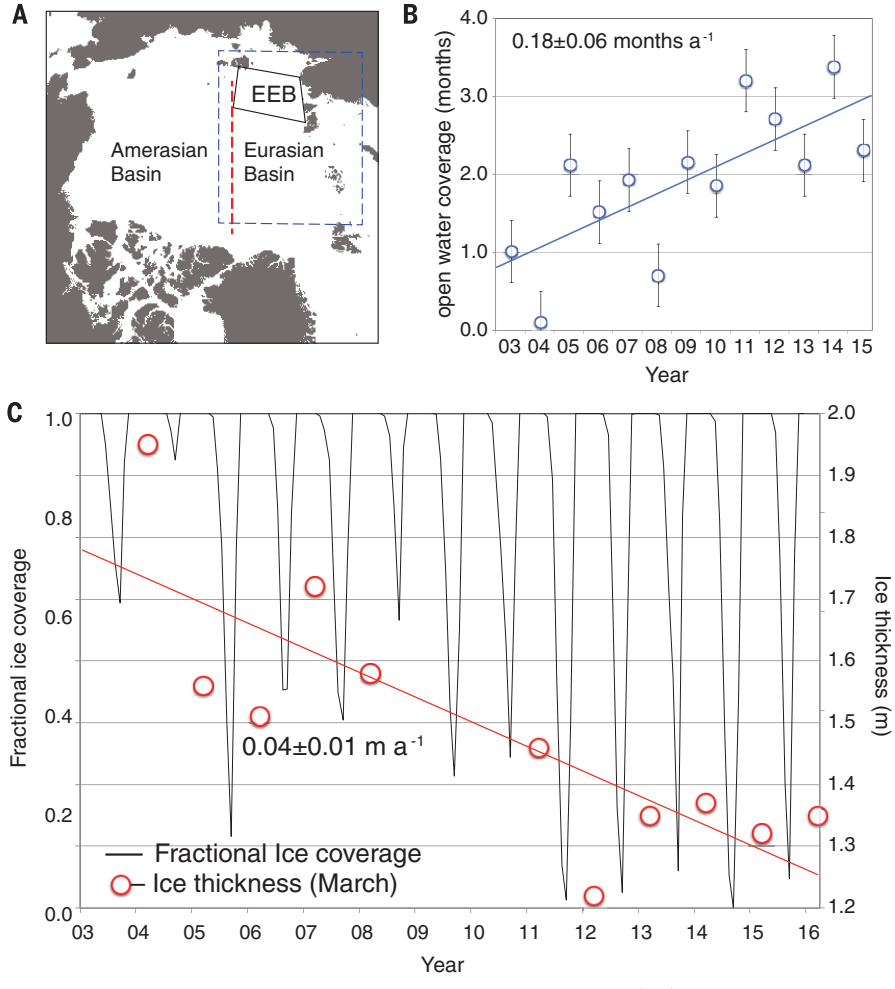

Fig. 1. Sea-ice fraction and thickness in the eastern Eurasian Basin (EB) since 2003. Sampling of the sea-ice state within the region [of 0.41 × 10^6 km^2, defined in (**A**)] shows a positive trend in annual open-water coverage [in months, integrated over a seasonal cycle, (**B**)]; this is accompanied by decreases in mean March ice thickness and monthly mean sea-ice coverage in (**C**) (measured as fraction of the total area). For the past five summers (2011 through 2015), the mean September ice coverage has been less than 10% ice coverage and seems to be approaching a seasonally ice-free state. Dashed box (in blue) shows the geographic coverage of the map in Fig. 2A, within the Arctic Basin. Red dashed line in (A) identifying the Lomonosov Ridge that separates the Amerasian and Eurasian basins.

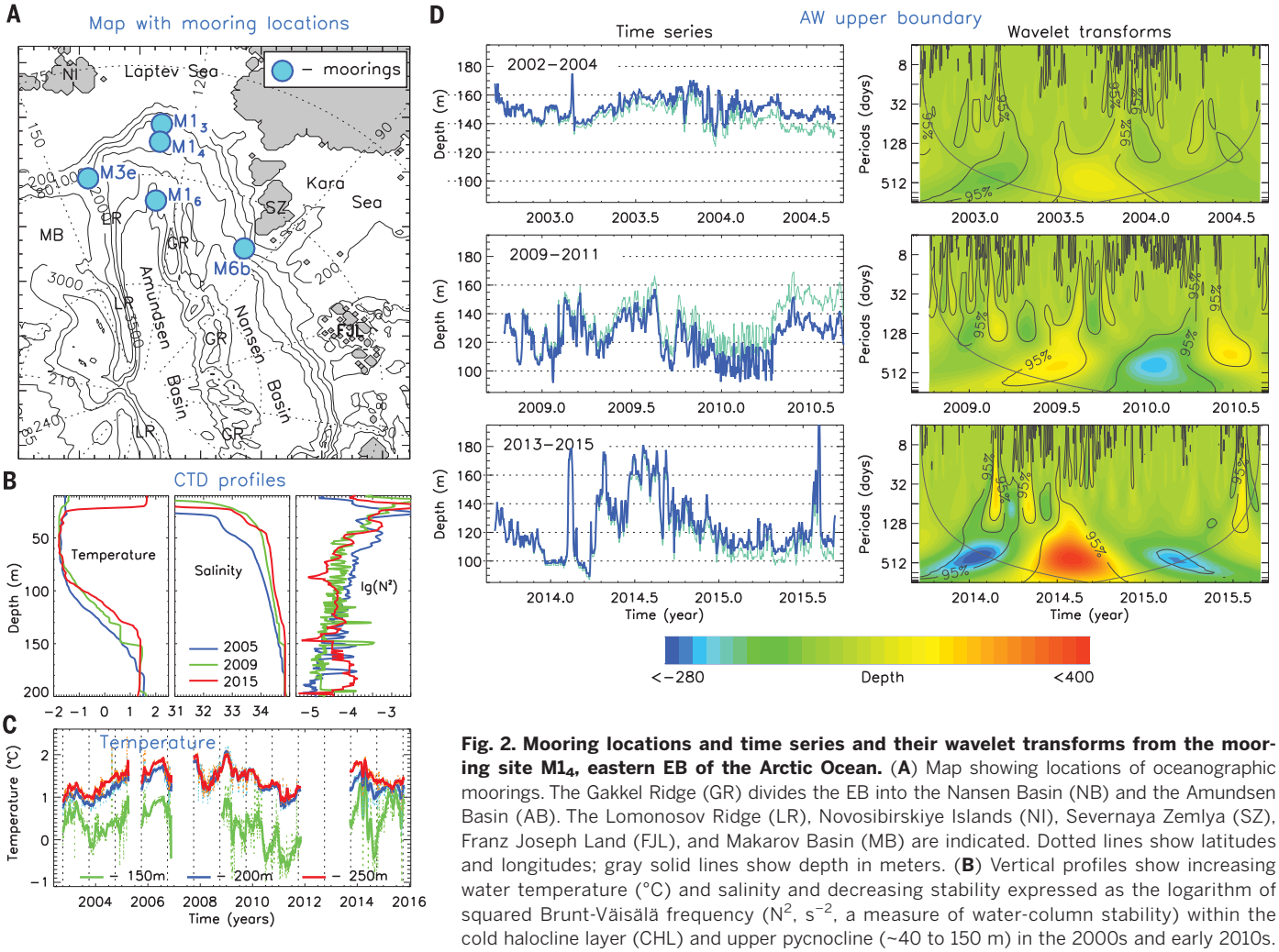

Fig. 2. Mooring locations and time series and their wavelet transforms from the mooring site $M1_4$, eastern EB of the Arctic Ocean. (**A**) Map showing locations of oceanographic moorings. The Gakkel Ridge (GR) divides the EB into the Nansen Basin (NB) and the Amundsen Basin (AB). The Lomonosov Ridge (LR), Novosibirskiye Islands (NI), Severnaya Zemlya (SZ), Franz Joseph Land (FJL), and Makarov Basin (MB) are indicated. Dotted lines show latitudes and longitudes; gray solid lines show depth in meters. (**B**) Vertical profiles show increasing water temperature (°C) and salinity and decreasing stability expressed as the logarithm of squared Brunt-Väisälä frequency (N^2, s^{-2}, a measure of water-column stability) within the cold halocline layer (CHL) and upper pycnocline (~40 to 150 m) in the 2000s and early 2010s. (**C**) Composite time series of water temperature (dotted lines for daily means, solid lines for monthly means). White segments indicate missing data. (**D**) Original (light blue) and detrended (dark blue) time series of the upper Atlantic water (AW) boundary (defined by 0°C isotherm, left) and wavelet transforms of detrended time series (right). In panels with wavelet transforms, 95% statistical significance and cones of influence are shown by gray lines.

(winter-to-summer) cooling in the CHL and upper pycnocline (65 to 130 m; see definition in the supplementary materials) is quantified using linear trends in Q. These trends (W m^{-2}) characterize the rate of change in Q and are equivalent to a divergent heat flux F_h (see definition in the supplementary materials). AW is the major source of heat for the layer underlying the CHL in this part of the Arctic Ocean. The seasonal mean F_h through the CHL and upper pycnocline inferred from these trends varies from 3.3 to 24.1 W m^{-2} (Table 1) (for reference, 1 W m^{-2} over a single year is equivalent to ~10 cm of ice loss).

Another potential contributor to the observed change in Q may be the lateral advection of heat. We argue, however, that the in-phase seasonal maxima and minima of wavelet transforms of Q as provided by all moorings (fig. S4), and the lack of any lag between Q calculated within separate overlying depth layers (not shown), each strongly suggest that the observed winter ventilation of the CHL and upper pycnocline is driven by surface cooling and sea-ice formation, not by lateral advection. Additional support for this statement comes from the wavelet analysis of Q records—not just from moorings $M1_3$ and $M1_6$ but from all six moorings deployed across the EB continental slope from 2013 to 2015 (see the supplementary materials for data description)—showing in-phase seasonal variations (not shown). The very different speeds of water transports across the slope, ranging from 13 cm/s (measured by 250- to 700-m shallow moorings) to 1 to 2 cm/s (measured at 2700 m and deeper mooring locations) make the in-phase pattern of the seasonal signal at all moorings impossible to explain using the advective mechanism. Moreover, the $M1_6$ mooring was placed in the ocean interior, well away from the intense heat transports associated with the near-slope boundary current, and yet data from this mooring yielded estimates for F_h consistent with estimates from other moorings deployed on the eastern EB continental slope.

Spatial averaging yields a seasonal mean F_h = 12.2 ± 3.8 W m^{-2} for winter 2013–2014 and 7.5 ± 0.8 W m^{-2} for winter 2014–2015 (Fig. 4 and Table 1). These inferred F_h values exceed previous estimates for upward heat fluxes of $O(3$ to 4) W m^{-2}, derived from 2007–2008 microstructure observations over the Laptev Sea slope (*29*) and 2009–2010 ITP-37 observations in the central Amundsen Basin (*14*) (Table 1), with new estimates for the same region being 2 to 4 times as high. We thus argue that AW shoaling, weakening of stratification, and warming of the upper pycnocline have led to seasonal upward AW heat fluxes never before observed in the eastern EB.

The inferred heat fluxes are equivalent to 54- and 40-cm reductions in ice growth over the 2013–2014 and 2014–2015 winter seasons, respectively, in the eastern EB (time intervals for seasons as defined by wavelet analysis) (fig. S4). The 2- to 4-fold increase in F_h since 2007–2008 explains up to 18 to 40 cm of sea-ice loss due solely to an increase in upward AW heat transport. These estimates are comparable to or even exceed ~18 cm in sea-ice loss attributed to atmospheric thermodynamic forcing and partially explain eastern EB sea-ice loss in recent years.

Sources of EB warm-water anomalies

Divergence of the Ekman transport (called Ekman pumping; see definition in the supplementary

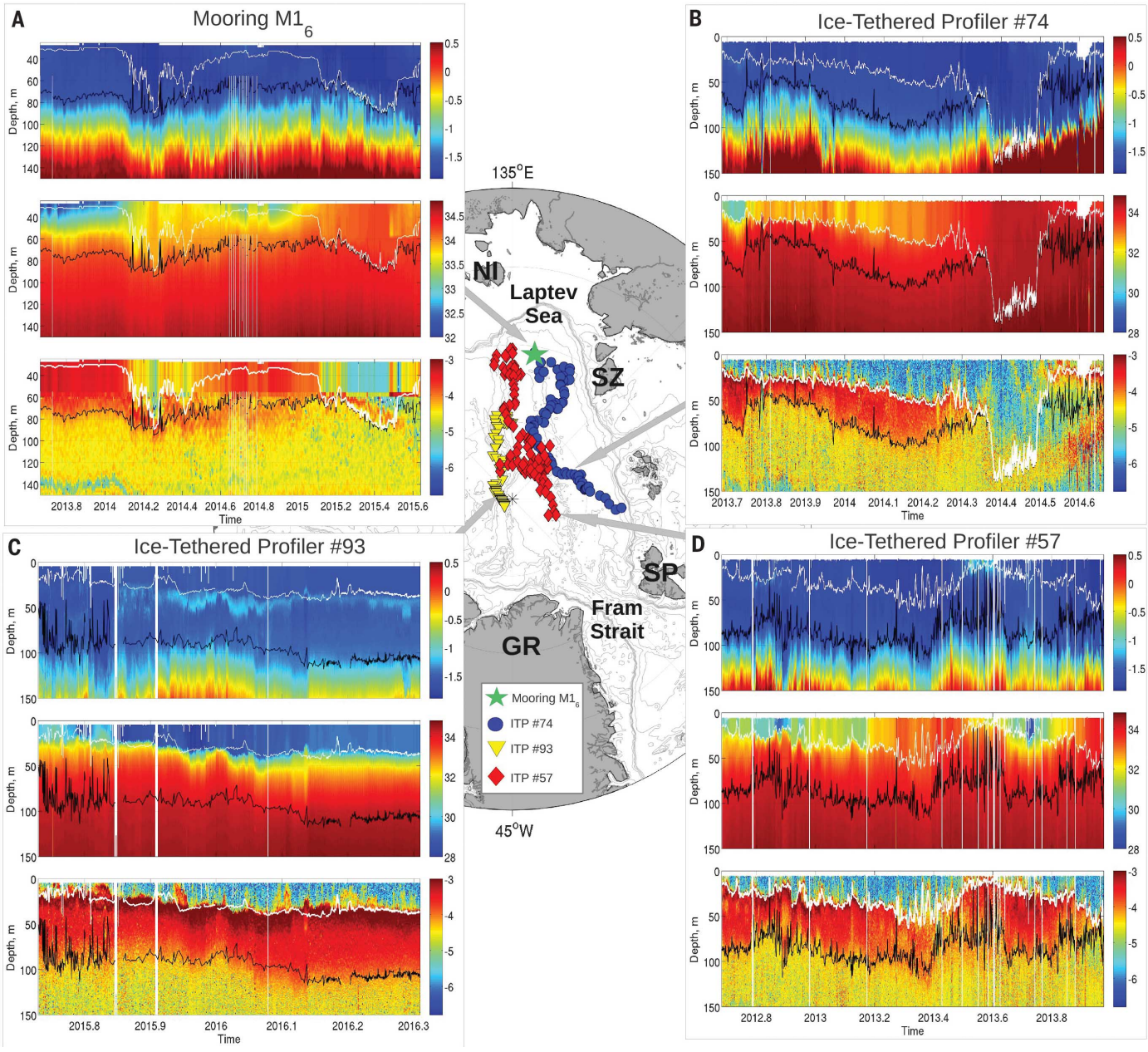

Fig. 3. Seasonal evolution of the upper ocean layers in the Eurasian Basin of the Arctic Ocean. (Top) Potential temperature (°C), (middle) salinity, and (bottom) logarithm of N^2 (s^{-2}) from (**A**) mooring and (**B** to **D**) along the Ice-Tethered Profiler drifts. White segments indicate missing data. White solid lines show the depth of the surface mixed layer (SML) and black solid lines show the depth of the underlying cold halocline layer (CHL) base; disappearance of the black line signifies disappearance of CHL and ventilation of the upper ocean.

materials) may be a local factor, which can cause shoaling of AW and its ventilation. However, our estimates suggest that Ekman pumping can explain only a 1.5-m seasonal shoaling of the AW and therefore does not contribute substantially to the anomalous state of the eastern EB in recent years (fig. S5).

Geochemical observations demonstrated that fresh shelf waters cross the Laptev Sea shelf break primarily at the Lomonosov Ridge–continental slope junction (*30*). Thus, although variations in atmospheric forcing have been shown to affect the storage or release of shelf waters (*30*) that affect stratification in the Amundsen Basin (*28*), such variations likely play only a minor role in the recent changes observed in the eastern EB.

We thus conclude that the source of changes associated with the AW in the eastern EB lies in processes beginning in upstream locations—namely, in Fram Strait and the western EB north of Svalbard. Similar to eastern EB observations, the vertical temperature difference in the upper ocean (>250 m) has been reduced in the area northeast of Svalbard since 2004 (fig. S6, D and E) due to warming in the upper part of the water column, mostly during winter. This trend is not present in data from Fram Strait, where the temperatures at both 75 and 250 m have changed very little (fig. S6, B and C).

One important difference between the eastern Fram Strait and the area northeast of Svalbard is that the eastern (inflow) side of Fram has been essentially ice-free year-round throughout recent history, whereas the slope north of Svalbard—beyond the Yermak Plateau—has traditionally been ice-covered most of the year. In recent decades, larger areas north of Svalbard have been ice-free for longer periods, primarily due to a contemporary increase in temperature of the AW inflow (*16*, *17*), similar to

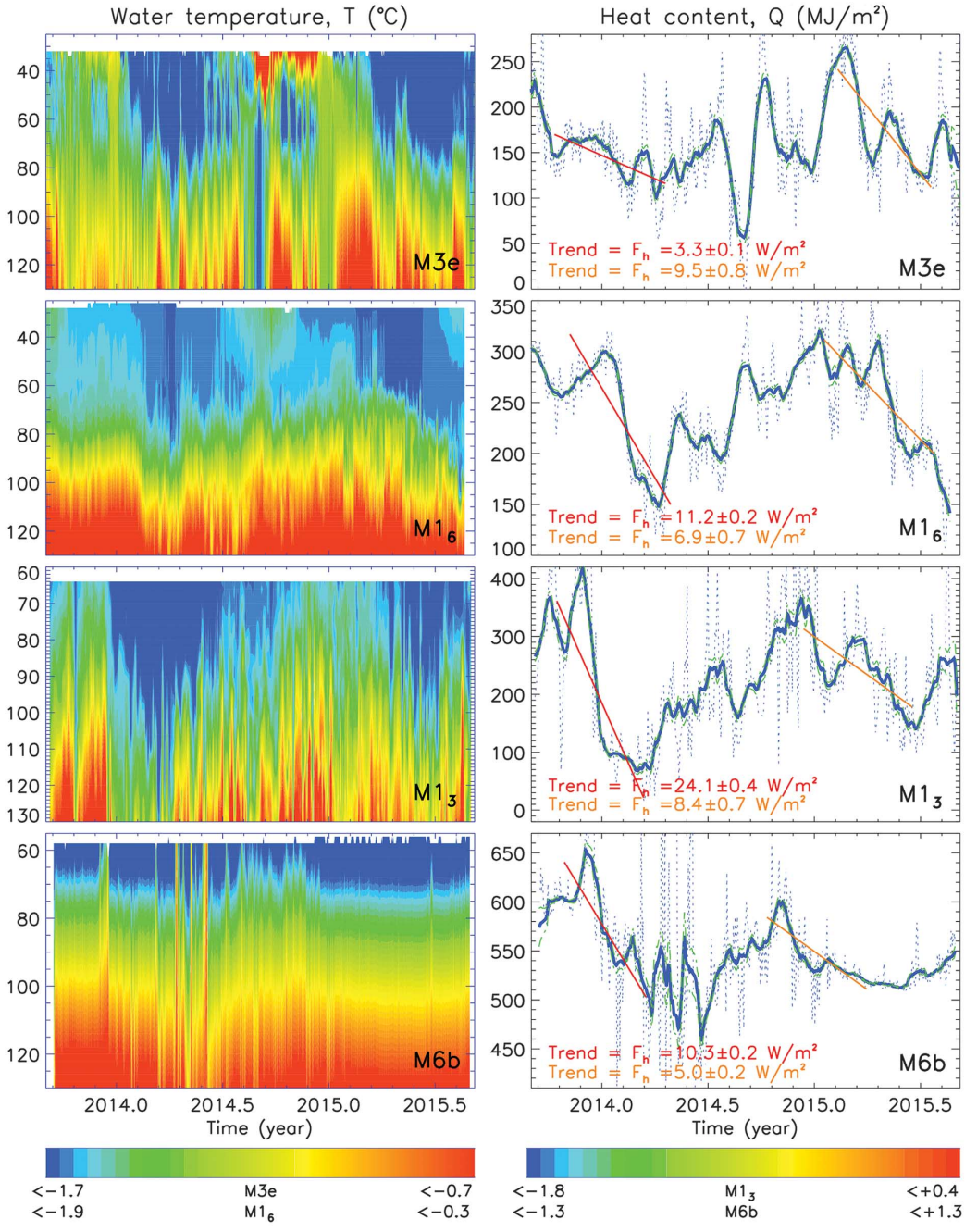

Fig. 4. Winter ventilation of the upper ocean in the eastern Eurasian Basin. (**Left**) Depth (m)–time distributions of temperature, *T*, and (**right**) time series of heat content, *Q*, (dotted blue lines, daily means; solid blue lines, monthly means; green dashed line, standard errors) for the 65- to 130-m layer (see mooring locations in Fig. 2). Maxima and minima of wavelet transforms were used to define the boundary of winter seasons (fig. S4). These boundaries were used to calculate trends in *Q* shown by red (winter 2013–2014) and orange (winter 2014–2015) lines. Slope of trends defines the rate of change of *Q* in time, which is equivalent to the divergent heat flux F_h (shown in red and orange).

the response in the Barents Sea to increased AW heat input there (*31*). During these extended ice-free periods over the slope north of Svalbard, enhanced local wind-driven generation and breaking of internal waves would be expected, as has been observed elsewhere in the Arctic (*32*). As a result, increased subsurface vertical mixing would tend to reduce the temperature gradient and increase *Q* above the temperature maximum in the AW inflow core, consistent with fig. S6, D and E. Additionally, the longer ice-free season over a larger area allows more solar radiation to be absorbed in the upper ocean, thus compensating to some degree for the increased local heat loss to the ice and atmosphere.

Discussion

This study provides evidence that the eastern EB is now in transition to conditions previously unique to the western Nansen Basin—an extension of more than 1500 km along the AW pathway from Fram Strait, as far as 125°E. The term "atlantification" is applied to the northward movement of sea ice in the Barents Sea, with attendant reductions in stratification, increased vertical mixing, and altered primary production (*33*, *34*). The recent extension of "atlantification" far into the EB, and the suite of associated processes, is shown conceptually in Fig. 5. The major driver for these changes is a powerful combination of processes associated with declining sea-ice cover and weakening of stratification in the layers over the AW. Gradual weakening of stratification in the eastern EB halocline began in at least the 1970s (*28*, *35*), providing the necessary preconditioning for a reconstruction of water mass structure. Weaker stratification and shoaling of the AW, together with net loss in ice volume, allow progressively deep winter ventilation in the eastern EB. This ventilation has resulted in enhanced upward AW heat fluxes, key to establishing the diminished sea-ice cover in the eastern EB during recent years.

Changes associated with "atlantification"—weakened stratification, increased vertical mixing, and sea-ice decline—will have dramatic effects on other geophysical and biogeochemical components

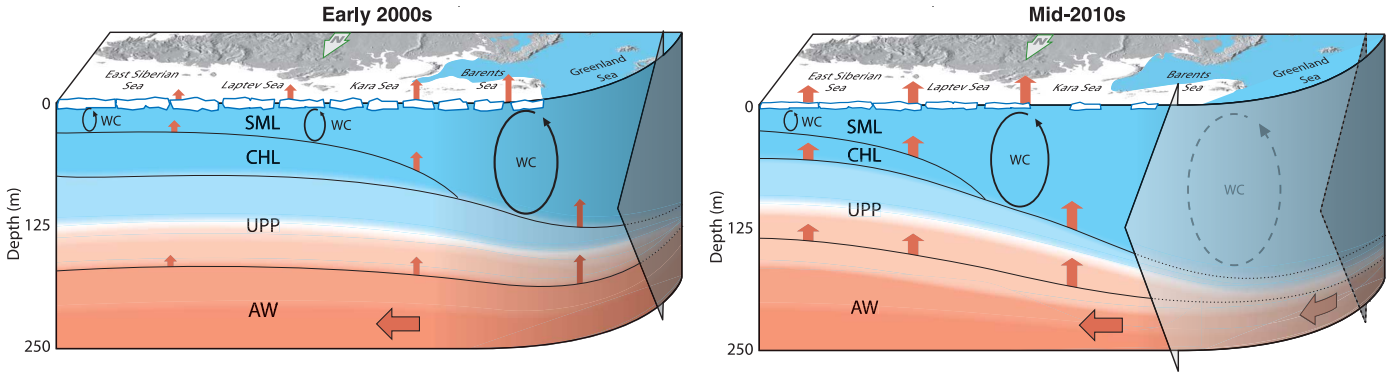

Fig. 5. Conceptual model of "atlantification" of the eastern EB continental margin in recent years. The broad arrow extending from the right side shows the encroachment of a suite of processes associated with "atlantification"; these are (i) increased penetration of surface signature of AW (increased flow, heat content, or both) into the eastern EB, (ii) reduction in ice cover resulting in (iii) greater surface heat and moisture flux and (iv) increased depth of winter penetrative convection, bringing additional heat and nutrients from AW into the Arctic surface water and transformation of the permanent cold halocline layer (CHL) to a seasonal halocline. SML and UPP indicate the surface mixed layer and upper permanent pycnocline. WC shows winter convection; red arrows indicate upward heat fluxes. Horizontal red arrows show inflows.

Table 1. Estimates of upward heat fluxes F_h (W/m^2).

Region	Topography	Depth level	F_h	Method	Source
Previous estimates, Eurasian Basin					
Yermak Plateau	Steep	Halocline	25	Microstructure profiles	(*46*)
Yermak Plateau	Steep	Ice-ocean interface	22	Turbulent flux buoy	(*47*)
North of Svalbard	Steep	Ice-ocean interface	*O*(100)	Eddy covariance,	(*48*)
		Halocline	*O*(100)	Microstructure profiles	
North of Svalbard	Slope	Halocline	2-4	Microstructure profiles	(*49*)
Laptev Sea	Slope	Above AW core (>250 m)	3	Microstructure profiles	(*29*)
Amundsen Basin	Interior	Upper CHL	0.05	Microstructure profiles	(*50*)
		SML	0.2		
Amundsen Basin	Interior	Between SML and AW core	3-4	ITP, heat content difference	(*14*)
Estimates from this study, eastern Eurasian Basin					
Eastern EB, off Severnaya Zemlya	Steep slope	Between SML and AW core	5.0-10.3	Heat content difference	M6b mooring
Eastern EB, central Laptev Sea, 125°E	Slope	Between SML and AW core	8.4-24.1	Heat content difference	$M1_3$ mooring
Eastern EB, 125°E	Interior	Between SML and AW core	6.9-11.2	Heat content difference	$M1_6$ mooring
Eastern EB, off Novosibirskiye Islands	Slope	Between SML and AW core	3.3-9.5	Heat content difference	M3e mooring

of the Arctic Ocean system. These include enhanced atmosphere-ocean interactions [with potential but highly debated mid-latitude consequences (*36*)], altered freshwater storage and export patterns within the Arctic Ocean (*37*), intensified shelf-basin exchange (*38*), increased primary production due to increased nutrient supply (*39*), and possibly changing the ocean's response to acidification due to the high buffering capacity of AW (*40*). Although specific physical mechanisms involved in sea-ice decline and upper ocean ventilation remain under debate (*5*), it is likely that higher-than-normal AW temperatures and salinities in the Nordic Seas, upstream of the Arctic Ocean gateways (*41*), will promote the further eastward "atlantification" of the polar basins. This follows with scenarios for regional ocean state responses to the climate changes proposed in (*42*) and has substantial effects for future changes in the Arctic Ocean and its sea-ice cover. The validity of extrapolating trends in the Arctic climate system into the future is affected, however, by the existence of large-amplitude, high-latitude variability (*43*–*45*). It is therefore imperative to apprehend how to separate climate trends and variability and to understand their nature in order to improve the accuracy of climate projections.

REFERENCES AND NOTES

1. D. K. Perovich *et al.*, *Ann. Glaciol.* **52**, 355–359 (2011).
2. D. K. Perovich *et al.*, *Geophys. Res. Lett.* **41**, 2019–2025 (2014).
3. J. M. Toole *et al.*, *J. Geophys. Res.* **115**, C10018 (2010).
4. K. Aagaard, L. K. Coachman, E. Carmack, *Deep-Sea Res. A, Oceanogr. Res. Pap.* **28**, 529–545 (1981).
5. E. C. Carmack *et al.*, *Bull. Am. Meteorol. Soc.* **96**, 2079–2105 (2015).
6. F. Nansen, *Sci. Results.* **9**, 427 (1902).
7. K. Aagaard, *Rapp. P.-V. Reun.- Cons. Int. Explor. Mer* **188**, 11–22 (1989).
8. B. Rudels, E. P. Jones, L. G. Anderson, G. Kattner, in *The Polar Oceans and Their Role in Shaping the Global Environment: The Nansen Centennial Volume*, AGU Geophysical Monograph vol. 85 (American Geophysical Union, Washington, DC, 1994), pp. 33–46.
9. Y. Aksenov *et al.*, *J. Geophys. Res.* **116**, C09017 (2011).
10. A. Pnyushkov *et al.*, *Deep Sea Res. Part I Oceanogr. Res. Pap.* **101**, 80–97 (2015).
11. D. A. Quadfasel, A. Sy, D. Wells, A. Tunik, *Nature* **350**, 385 (1991).
12. E. C. Carmack, R. W. Macdonald, R. G. Perkin, F. A. McLaughlin, R. J. Pearson, *Geophys. Res. Lett.* **22**, 1061–1064 (1995).
13. I. V. Polyakov *et al.*, *Geophys. Res. Lett.* **32**, L17605 (2005).
14. I. V. Polyakov *et al.*, *J. Phys. Oceanogr.* **43**, 2142–2155 (2013).
15. V. Ivanov *et al.*, *J. Phys. Oceanogr.* **46**, 1437–1456 (2016).
16. V. V. Ivanov, V. A. Alexeev, I. Repina, N. V. Koldunov, A. Smirnov, *Adv. Meteorol.* **2012**, 201818 (2012).
17. I. H. Onarheim, L. H. Smedsrud, R. B. Ingvaldsen, F. Nilsen, *Tellus* **66**, 23933 (2014).
18. D. G. Vaughan *et al.*, in *Climate Change 2013* (Cambridge Univ. Press, Cambridge, UK and New York, NY, USA, 2013), pp. 317–382.
19. R. Kwok, D. A. Rothrock, *Geophys. Res. Lett.* **36**, L15501 (2009).
20. R. Kwok, G. F. Cunningham, *Phil. Trans. R. Soc. A.* **373**, 20140157 (2015).
21. I. V. Polyakov, J. Walsh, R. Kwok, *Bull. Am. Meteorol. Soc.* **93**, 145–151 (2012).
22. Sea Ice Prediction Network (SIPN), Post-Season Report; https://www.arcus.org/sipn/sea-ice-outlook/2016/post-season#two (2016).
23. C. Li, B. Stevens, J. Marotzke, *Geophys. Res. Lett.* **42**, 8131–8139 (2015).
24. R. Krishfield, J. Toole, A. Proshutinsky, M.-L. Timmermans, *J. Oceanic Atmos. Tech.* **25**, 2091 (2008).

25. I. A. Dmitrenko *et al*., *J. Geophys. Res.* **114**, C06010 (2009).
26. B. Rudels, L. G. Anderson, E. P. Jones, *J. Geophys. Res.* **101**, 8807–8821 (1996).
27. B. Rudels, P. Jones, U. Schauer, P. Eriksson, *Polar Res.* **23**, 181–208 (2004).
28. M. Steele, T. Boyd, *J. Geophys. Res. Oceans* **103**, 10419–10435 (1998).
29. Y.-D. Lenn *et al*., *Geophys. Res. Lett.* **36**, L05601 (2009).
30. D. Bauch *et al*., *J. Geophys. Res.* **114**, C05008 (2009).
31. M. Årthun, T. Eldevik, L.-H. Smedsrud, Ø. Skagseth, R. B. Ingvaldsen, *J. Clim.* **25**, 4736–4743 (2012).
32. L. Rainville, R. A. Woodgate, *Geophys. Res. Lett.* **36**, L23604 (2009).
33. M. Reigstad, P. Wassmann, C. W. Riser, S. Øygarden, F. Rey, *J. Mar. Syst.* **38**, 9–29 (2002).
34. P. Wassmann *et al*., in *The Organic Carbon Cycle in the Arctic Ocean*, R. Stein, R. W. Macdonald, Eds. (Springer-Verlag Heidelberg-Berlin-New York, 2004), pp. 101–138.
35. I. V. Polyakov *et al*., *J. Phys. Oceanogr.* **40**, 2743–2756 (2010).
36. J. Cohen *et al*., *Nat. Geosci.* **7**, 627–637 (2014).
37. E. C. Carmack *et al*., *J. Geophys. Res.* **121**, 675–717 (2016).
38. W. Williams, C. E. Carmack, *Prog. Oceanogr.* **139**, 24–41 (2015).
39. B. A. Bluhm, K. N. Kosobokoba, E. C. Carmack, *Prog. Oceanogr.* **139**, 89–121 (2015).
40. M. Yamamoto-Kawai, F. McLaughlin, E. C. Carmack, *J. Geophys. Res. Oceans* **118**, 6274–6284 (2013).
41. K. M. H. Larsen, C. Gonzalez-Pola, P. Fratantoni, A. Beszczynska-Möller, S. L. Hughes, Eds., *ICES Report on Ocean Climate 2015. ICES Cooperative Research Report No. 331* (International Council for the Exploration of the Sea, Copenhagen, 2016).
42. K. Aagaard, E. C. Carmack, in *The Polar Oceans and Their Role in Shaping the Global Environment*, *Geophys. Monogr. Ser.*, vol. 85, O. M. Johannessen, R. D. Muench, J. E. Overland, Eds. (AGU, Washington, DC, 1994), pp. 5–20.
43. I. V. Polyakov *et al*., *Ecol. Appl.* **23**, 1745–1764 (2013).
44. A. Proshutinsky, D. Dukhovskoy, M.-L. Timmermans, R. Krishfield, J. L. Bamber, *Phil. Trans. A.* **373**, 20140160 (2015).
45. R. Zhang, *Proc. Natl. Acad. Sci. U.S.A.* **112**, 4570–4575 (2015).
46. L. Padman, T. M. Dillon, *J. Geophys. Res.* **96**, 4769–4782 (1991).
47. M. G. McPhee, T. Kikuchi, J. H. Morison, T. P. Stanton, *Geophys. Res. Lett.* **30**, 2274 (2003).
48. A. Sirevaag, I. Fer, *J. Phys. Oceanogr.* **39**, 3049–3069 (2009).
49. I. Fer, R. Skogseth, F. Geyer, *J. Phys. Oceanogr.* **40**, 1613–1630 (2010).
50. I. Fer, *Atmos. Ocean. Sci. Lett.* **2**, 148–152 (2009).

ACKNOWLEDGMENTS

This study was supported by NSF grants 1203473 and 1249133 (A.V.P., I.V.P., M.B.A., R.R., and V.V.I.), National Oceanic and Atmospheric Administration grant NA15OAR4310155 (A.V.P., I.V.P., M.B.A., R.R., T.M.B., and V.V.I.), Russian Science Foundation grant 14-37-00053, and by the A-TWAIN project, funded by the Arctic Ocean program at the FRAM-High North Research Centre for Climate and the Environment. We thank Henriksen Shipping Service AS, for help with logistics. The mooring recovery and deployment was a great team effort by all onboard the research vessels *Akademik Fedorov* (2013) and *Akademik Tryoshnikov* (2015). We thank our colleagues from the Arctic and Antarctic Research Institute, Russia, particularly V. Vizitov, V. Zaitsev, and E. Morozova, for their help with cruise preparations. All mooring data used in this study are available on the web at https://arcticdata.io/catalog/#view/arctic-data.7792.4. All authors participated in data processing and preliminary analysis; A.V.P., I.M.A., I.V.P., R.R., and V.V.I. carried out statistical analysis of data; R.Kw. provided sea-ice information and processing; T.K. processed Fram Strait data; A.S. provided processing and analysis for Svalbard mooring data; A.Y. analyzed fast-ice thickness data; and T.M.B. worked with reanalysis data. All authors contributed to interpreting the data and writing the paper. The authors declare no competing financial interests.

SUPPLEMENTARY MATERIALS

www.sciencemag.org/content/356/6335/285/suppl/DC1
Materials and Methods
Supplementary Text
Figs. S1 to S6
Table S1
References (*51*–*57*)

16 August 2016; accepted 24 March 2017
Published online 6 April 2017
10.1126/science.aai8204

Greater role for Atlantic inflows on sea-ice loss in the Eurasian Basin of the Arctic Ocean

Igor V. Polyakov, Andrey V. Pnyushkov, Matthew B. Alkire, Igor M. Ashik, Till M. Baumann, Eddy C. Carmack, Ilona Goszczko, John Guthrie, Vladimir V. Ivanov, Torsten Kanzow, Richard Krishfield, Ronald Kwok, Arild Sundfjord, James Morison, Robert Rember and Alexander Yulin

Science **356** (6335), 285-291.
DOI: 10.1126/science.aai8204originally published online April 6, 2017

Losing its character

The eastern Eurasian Basin of the Arctic Ocean is on the far side of the North Pole from the Atlantic, but it is becoming more like its larger neighbor as the climate warms. Polyakov *et al.* show that this region is also evolving toward a state of weakened stratification with increased vertical mixing, release of oceanic heat, and less sea ice. These changes could have considerable impacts on other geophysical and biogeochemical aspects of the Arctic Ocean system and presage a fundamentally new Arctic climate state.

Science, this issue p. 285